Solid Freeform Fabrication 2017: Proceedings of the 28th Annual International
Solid Freeform Fabrication Symposium – An Additive Manufacturing Conference
Reviewed Paper

ACTIVE - Z PRINTING: A NEW APPROACH TO INCREASING3D PRINTED PART STRENGTH

Jivtesh B. Khurana[*], Shantanab Dinda[†], and Timothy W. Simpson[*†]
[*]Department of Mechanical and Nuclear Engineering
[†]Department of Industrial and Manufacturing Engineering
The Pennsylvania State University, University Park, PA, 16802

Abstract

Research suggests that topology and build parameters in Fused Filament Fabrication (FFF) play a vital role in determining mechanical properties of parts produced by this technique. In particular, the use of 2D layers printed parallel to the build surface produces high anisotropy in parts making them the weakest when loaded perpendicular to the layer interfaces. We investigate a novel approach that uses non-planar 3D layer shapes - Active Z printing, to improve mechanical strength through alignment of localized stress tensors parallel to the deposition paths. Sinusoidal layer shapes are used with varying amplitude, frequency, and orientation. Design of experiments is performed to correlate effect of varying shape and orientation of sinusoidal layer shapes on flexural strength of parts. Based on this, the results are used to decide parameters to be studied further and characterize their effect on the strength of parts.

1. Introduction

Additive Manufacturing (AM) is the process of creating end use parts by adding material in a layer by layer manner. Fused Filament Fabrication (FFF) is a process, where a thermoplastic is melted into liquid state in an extruder head and subsequently deposited through a nozzle. This nozzle traces the part's cross-sectional geometry to produce 3D parts directly from CAD data in a layer by layer manner[1]. The layers used in this process are conventionally two dimensional, and printed parallel to the build surface. As a consequence of this layer by layer approach, polymer parts produced by FFF are anisotropic, making them especially weak at the interface between adjacent layers and deposition toolpaths[1,2,3].

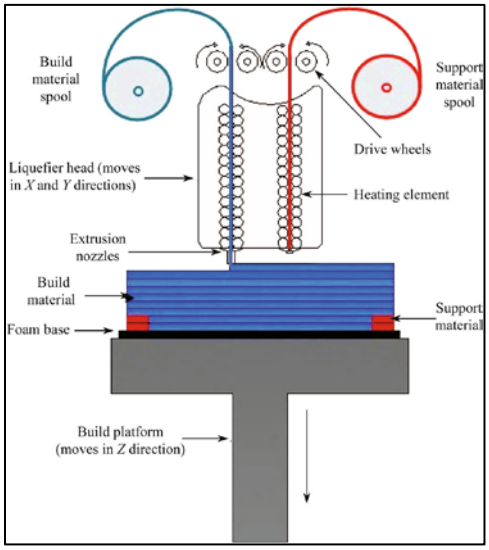

Figure 1: Fused Filament Fabrication Process

Fused Filament Fabrication (FFF) using 2D layers have been extensively investigated to improve the mechanical properties through optimization of process parameters[1]. In the past, researchers have explored the idea of non-planar deposition paths through the study of Curved Layer FFF (CLFFF). Active-Z includes the use of dynamic tool paths that contain Z movements within individual layers, as compared to conventional FFF toolpath that have constant Z values in intra-layer extrusions.

Active – Z printing uses distinct layer shapes oriented relative to a part in order to produce improvement in flexural properties of parts produced using AM. An open source slicer, *Bread*, was used which accepts part geometry and layer shape as an STL file and produced Gcode that can be interpreted by a 3D printing machine. The Gcode produced is further post processed in order to remove unwanted travel moves, nozzle to part collisions and optimize travel moves to reduce print time. We used a *Rostock Max V2 Delta* 3D printer due to its capability to produce smooth and rapid Z movements. The machine interface was performed using *Printrun Pronterface* software which is also open-source. All flexural specimens were produced in the XYZ orientation with infill toolpath orientations alternating $0^o/90^o$ from the Y -axis of the machine. Flexural testing was performed following the procedure outlined in ASTM D790 and data was collected for the experimental design.

2. Literature Review

2.1 Modeling and effect of Curved Layer Fused Filament Fabrication

Curved Layer Fused Filament Fabrication (CLFFF) was introduced by Chakraborty et al. to improve mechanical properties, and reduce stair stepping and print time. Their approach uses offsetting of part surfaces using Bezier surfaces to create 3D layers[7], however, no physical tests were conducted. Singamneni et al. proposed another technique that used generation of surface point data from STL files and then offsetting points in the Z direction, followed by taking a cross product of 2 vectors at every surface point[4]. Parts produced by this technique were subjected to flexural loading, resulting in a 40% increase in load before fracture when compared with conventional parts showing potential for strength improvement using CFFF. Huang et al. studied the effect of varying raster angle on the flexural properties and concluded that strength decreases with increasing raster angle, however, this relation is non-linear[5]. They also developed an adaptive slicing method to vary layer height for CLFFF, tests showed improved resolution of fine and sharply varying surface profiles as well as direct relation between flexural strength and layer thickness[8]. Furthermore, Yerazunis et al. used hemispherical-shaped specimens to test CLFFF parts in shear and bending, and concluded that parts produced using CLFFF are 3.5 to 5 times the strength of conventionally printed parts[6].

Another major application of CLFFF has been towards recreating skins and surfaces of parts with small curvature. Conventional Flat Layer Fused Filament Fabrication (FLFFF) produces stair-stepping and inferior mechanical properties, this can be easily rectified using CLFFF. Llewellyn-Jones et al. conducted case studies using shell like geometries of shoe in-sole, dished sandwich panel and a car body panel[9]. Using these case studies, they showed that it was possible to combine curved layer and conventional statics Z layers to produce superior surface finish and minimize risk of part failure from layer delamination. Similar studies were conducted by Allen et al. on using curved toolpath for skin of parts. Innovative slicing and printing methods were implemented and an improvement in supported surface quality was observed. They suggested that these techniques provide improvements in mechanical properties, however, physical studies have not been conducted[10]. An analogous process was implemented for concrete panels by Lim

et al. They improve surface finish by minimizing staircase effect, reduced printing time by minimizing layer count, and increased filament bonding by minimizing voids and maximizing the contact area between layers[11].

2.2 AM Process - Property – Structure Relationships

Identification of Process-Property-Structure are imperative for every manufacturing process; especially in AM, where anisotropic properties can emerge due to factors such as material deposition pattern, build orientation and material interface. It is known that processing parameters affect fiber to fiber bond strength and mesostructure of parts. Furthermore, uneven thermal cycles due to layered deposition leads to accumulation of stresses, causing distortion which is primarily responsible for poor interlayer bonding, subsequently reducing strength (Section 2.1).

Existing research has shown that processing parameters play an important role in providing optimum conditions for strength development in FFF processed parts. These are raster angle, raster width, layer thickness, air gap, part orientation, contour width, and extrusion & envelope temperatures. Es-Said et al. showed that molecules align themselves in the direction of raster deposition causing decrease in resistance to flexural load, hence, decreasing flexural strength with increasing raster angle[13]. Similar experiments for raster angle conducted by Constance et al. found the same relation, however, failure surface showed shear failure at large raster angles. These effects contribute to increased resistance to load due to long raster lengths associated with small raster angles[14]. Ahn et al. found that raster angle and air gap significantly contributed to tensile and flexural strength as compared to raster width, model temperature, and filament color using a fractional factorial experimental design[1]. Moreover, Sood et al. varied layer thickness, build orientation, raster angle, raster width, and air gap using a central composite experiment design and analyzed their relationships to tensile, compressive, and flexural strength using response surface methodology. They found that reduction in distortion and increase in inter-extrusion diffusion caused increase in strength. These effects were primarily seen with large raster widths, large number of layers produced as a result of combination of layer heights and part orientation[15, 16]. Further, small values of air gap and raster angle favored high strength similar to the results by Ahn et al. and Es-Said et al.; Wang et al. optimized flexural modulus for complaint bow structure using a L_9 orthogonal taguchi array. It was found that air gap influenced the modulus the most followed by raster angle, raster width, and slice height[17].

Apart from working parameters, machine parameters such as extrusion temperature, envelope temperature, nozzle diameter, and feed-rate also play a vital role in determining strength of parts. As the extruded plastic cools, internal stresses are developed due to uneven deposition speeds resulting in layer deformation in the form of warping, cracking, and layer de-lamination. These phenomena greatly affect part strength and dimensional accuracy[18]. Moreover, it was determined that these deformations increase with increasing model height. However, these deformities can be eradicated by increasing chamber temperature to the glass transition temperature of the deposition material. Bellehumeur et al. used the polymer sintering model to evaluate the effects of extrusion and envelope temperatures, and dimensions of the extruded

filaments. Extrusion temperature plays a vital role in neck growth of the bonding zone as temperature cannot be maintained for long durations for bonding between filaments to complete. As a result, mechanical properties of the bonding zone are inferior to virgin ABS material[19].

Bellehumeur et al. further found that temperature at bottom layers rises above the glass transition temperature and rapidly decreases in the direction of movement of extrusion head. This temperature increases with the number of layers; hence bottom layer extrusions experience higher diffusion as compared to the rest of the part[20]. Joseph et al. used polymer rheology data and polymer weld theory to predict strength of parts subject to uniaxial tension. It was found that inter-extrusion bond was fully healed. Based on these results, the strength was predicted to be slightly over the 95% confidence level of experimental strength[21].

2.3 Research Scope

Although, CLFFF has been modeled and demonstrated, the applications of non-planar sinusoidal layers are yet to be modeled and studied. Active-Z printing provides the ability to define sinusoidal layer geometry in order to precisely vary material properties inside a part. Given that mechanical properties of parts are closely linked to layer shape and orientation, achieving an apt understanding of how part properties relate to process parameters is paramount to ensure its relevance and reliability as an AM process.

In this paper, the authors seek to probe the process-property-structure relationships of Active-Z printing through a design of experiments. A fractional factorial design is used to analyze the effect of five parameters on the flexural strength and modulus of specimens, (i) Amplitude/Pitch ratio (layer shape), (ii) Z-Rotational angle, (iii) X-Rotational Angle, (iv) layer height, (v) and air gap. The research question is "***Do non-planar sinusoidal layer shapes cause an increase in the flexural strength and modulus of parts produced using Active-Z printing? If so which factors significantly affect them?***" Active-Z Printing is explained in detail in section 3. The experimental design is outlined in section 4 followed by results and discussions in section 5 & 6 respectively.

3. Active-Z Printing

Active-Z printing is a branch of FFF technique which involves the use of motion in X, Y, Z axis simultaneously to produce shapes with 3D cross-sectional area. This is contrary to conventional FFF which only uses planar layers. Active-Z printing can be divided into two design tracks, first, the design of desired part and second, design of layers. The design of layers allows designers to effectively control the material behavior of the part in addition to the geometry. A process workflow for using Active-Z is shown in figure 2. In this study, a sinusoidal herringbone structure is used as a layer shapes. These herringbone structures were inspired by bio-structures investigated by Yaraghi et al. who found sinusoidal herringbone structures in dactyl club of a mantis shrimp[25]. These geometries were found to have increased young's modulus and fracture strains as compared flat helicoidal structures.

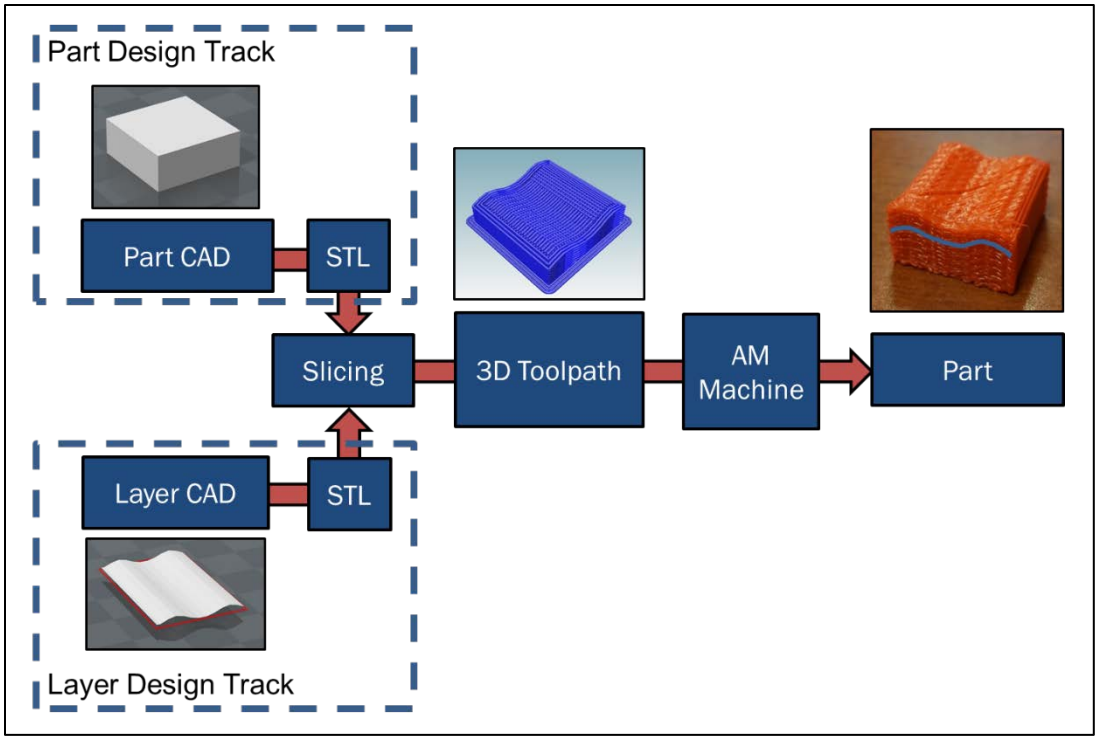

Figure 2 : Design workflow for Active-Z Printing

In order to slice layers in such a shape an open source slicer, *Bread*[23], is used which accepts (i) the part to be sliced as an STL, (ii) the shape of the layer as an STL, (iii) and a configuration file highlighting the process parameters used to manufacture the part. The slicer exports toolpath as G-code which can be readily accepted by AM machines. However, the slicing software is under development and is prone to producing a range of unwanted travel moves which lengthen print time as well as cause collisions between the nozzle and the specimen to be printed. A MATLAB script was used to remove unwanted travel moves, check for nozzle-part collision and create fast and optimum travel path.

4. Experimental Design and Methods

4.1 Parameter Selection

Mechanical properties of FFF parts are closely linked to processing parameters like orientation, extrusion width, raster angle, layer height, and air gap. Further, strength development between individual roads is highly dependent on the extrusion temperature and scan speed (Section 2.2). With the induction of Active-Z printing the authors feel that the part's mechanical properties might be affected by layer's shape and orientation. While raster angle has been shown to affect CLFFF parts, the layer shape and orientation has not yet been studied.

A fractional factorial test has been used by the authors to characterize the effect of layer shape and orientation in the Active Z process. A cause and affect diagram (aka Ishikawa diagram) was created to group factors that affect strength of 3D printed parts and is shown in figure 3. The purpose of cause and affect diagrams is to systematically group causes of specific event into families leading to identification of the family containing the root cause.

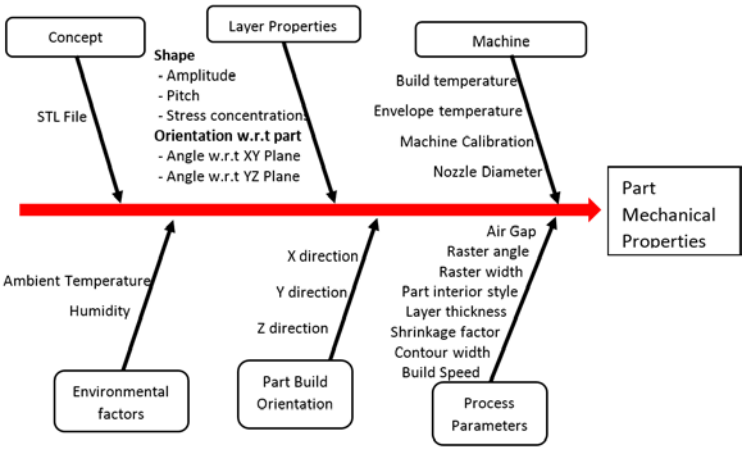

Figure 3: Cause and effect diagram from FFF

Although all branches of the Ishikawa Diagram show the factors that could affect the material properties of the specimen, the "Layer Properties" and "Process Parameter" branch was further analyzed due to its uniqueness to Active-Z. Figure 4 depicts the 5 parameters chosen for analysis. The description and hypothesized effect for each parameter is shown in Table 1.

Table 1: List of parameters used for design of experiments

Parameter	
Air gap	***Description:*** In-plane distance between two adjacent extrusions in a cross section of a layer ***Hypothesis:*** Varying air gap directly effects part density and thus strength decreases with increasing air gap.
Amplitude/pitch	***Description:*** A measure of the shape of sinusoid, a large ratio signifies a thin and stretched out shape while a small ratio signifies fat and bulged shape. ***Hypothesis****:* The sinusoids act like springs; the ratio would be directly proportional to stiffness of part. Further, load applied is resolved into a normal and shear load due to varying shape of part.
Z- Rotation angle	***Description****:* It is the angle between the x-axis of layer and the x-axis of the part measured counter clockwise from the part's x-axis. ***Hypothesis****:* Small angles would result a larger road length increasing resistance to load.
X- Rotation angle	***Description****:* It is the angle between the normal vector of layer shape and z-axis of the part measured clockwise from the part's z-axis. ***Hypothesis****:* Increase in angle would result in a further distribution of load along layer normal and layer parallel vectors, thus increasing strength.
Layer height	***Description****:* The thickness of each layer used to build the part, it is often an integral multiple of the size of part. ***Hypothesis****:* It is know that flexural strength increases with increasing layer height[15], interaction with layer shape would cause increased strength.

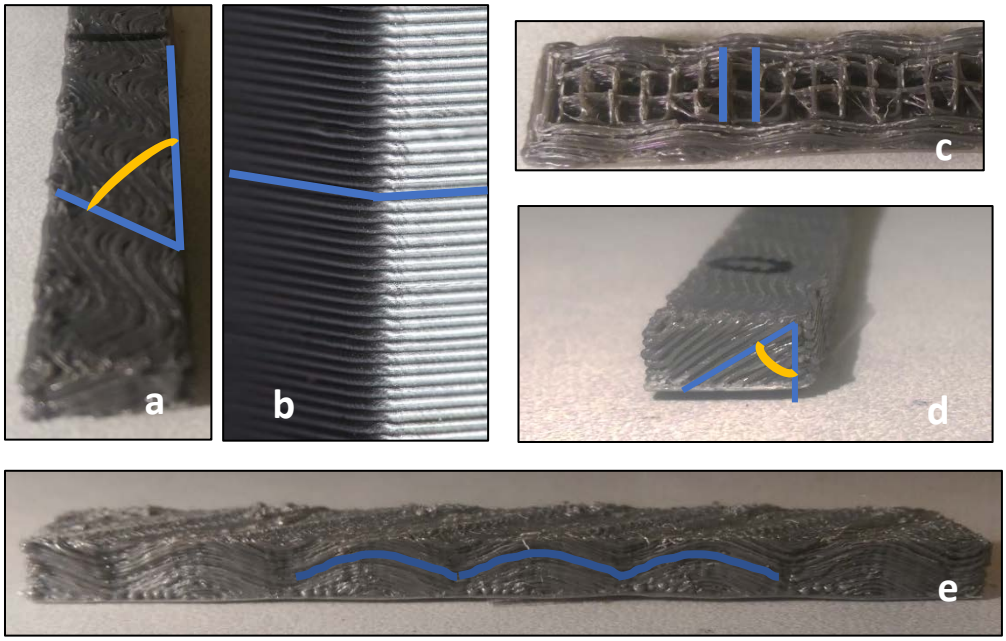

Figure 4: List of parameters tested. (a) Z Rotation Angle (b) Layer Height (c) Air gap (d) X Rotation Angle (e) Amplitude/pitch

4.2 Design of Experiments

The goal of the experiment is to identify parameters that affect the flexural strength and modulus of parts created using Active-Z Printing. Theories introduced in Design and Analysis of Experiments[24] are consulted to produce a 5 parameter 2 level fraction factorial design of experiments (DOE). A linear relationship between the response and the five parameters was desired, hence, only 2 levels one set high (+1), one set low (-1) was chosen. Appropriate level of each parameter was decided based on nozzle shape, machine limitations and literature review.

A half factorial experimental design was devised for the study. A defining relation of E = ABCD was chosen and higher order effects were confounded with main and second level interaction effects. This allows us to run 16 distinct tests with each test replicated thrice to quantify standard error within each experiment. As a result, a total of 48 test specimen were used, making the DOE relatively easy to regulate and execute. A list of coded parameters in the factorial designed experiment is shown in table 2.

Table 2: Process parameters tested and their respective testing levels

Symbol	Parameter	Unit	Level -1	Level 1
A	Air Gap	mm	1.25	3
B	Amplitude/Pitch Ratio	N/A	0.09858	0.14997
C	X-Rotational angle	Degree	30	60
D	Z-Rotational angle	Degree	60	75
E	Layer Height	Mm	0.3	0.4

4.3 Experimental Procedure

ASTM D790-15e2 was followed to measure specimens' flexural strength and modulus. This standard has been used in engineering design and allows comparison of material properties across manufacturing platforms, including existing AM processes. Figure 5 summarizes dimensions for the selected flexural test specimen. A length of 96mm was used with a thickness of 6mm and a width of 12mm. This allows for an 80mm span with 8mm overhang and a span to depth ratio of 13.33:1. Specimens' lengths and widths were measured to monitor any variability in size. Due to the experimental nature of the slicing algorithm and the nozzle geometry, it was found that the specimen's dimensions were 12.96 ± 0.504 mm wide and 6.03 ± 0.145 mm thick. Similarly, the specimens' masses were measured on a digital scale to monitor to variation in mass, found to be ± 1g.

Each experiment (table 3) was printed in the run order using a SeeMeCNC Rostock Max V2. Parts were printed at a uniform speed of 30mm/s with an extrusion temperature of 210 ± 2º C and a bed temperature of 105 ± 1 º C, as recommended by the filament manufacturer. All temperature measurements were taken using a 100K EPCOS thermistors rated for temperature measurement up to 300º C. Each specimen was printed individually, a total of 48 build trays were printed in this study with each specimen in the XYZ orientation. Following the completed print job, the build plate was allowed to cool down from 105 ± 2º C to 65 ± 2º C before the specimens were removed to minimize warping. Upon removal, the specimens were stored in an airtight transparent bag in a metal cabinet located away from potential sources of moisture.

Tensile tests were conducted using an MTS 800 material testing machine in accordance to ASTM D790 standard. Using TestWorks for data acquisition with the machine, tests were conducted at a stable environment of 25 º C, 25 - 50% humidity and tested at a crosshead federate of 1.78 mm/min until specimens ruptured on the tensile load side. Specimen deflection was measured using crosshead position in accordance to the D790 Standard testing procedure type I.

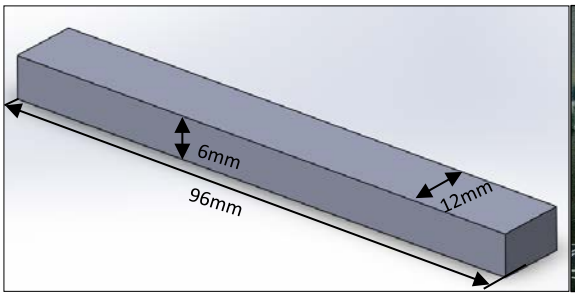

Figure 5: Size of the test specimen used for flexural testing

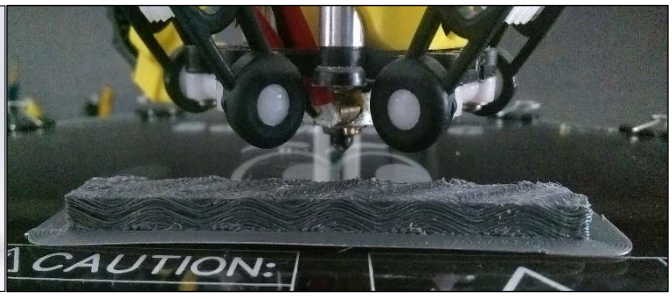

Figure 6: Printed specimen showing sinusoidal layer shape

5. Results and Statistical Analysis

5.1 Experimental Data

The results were obtained from flexural testing of all 16 specimens with 3 replicates each. The mean and standard deviation of each experiment is summarized in table 3. To perform statistical analysis on the data obtained, the assumptions made for the analysis of the factorial design are first verified. A normal probability of the runs was calculated for Flexural Strength and modulus. This follows a linear trend, indicating that the data is an acceptable normal probability distribution with a confidence of 96.4% and 97.1% for flexural strength and modulus respectively. Further, an outlier analysis was performed on the dataset to find datasets that lies an abnormally large distance away from other random samples in a population. For the flexural strength, no outliers exist, however, the flexural modulus does show an outlier (Experiment Id 3) but it can be ignored given there were replicates for each specimen. This outlier would add to the pure error of the model.

Finally, a residual analysis was conducted for both flexural strength and modulus. Residuals for each portray a normal distribution, versus fits and versus order plots show a balanced response and the run order does not show any time sequence. The authors can conclude that a linear model would be adequate for the analysis and accounts for all influences on strength and modulus.

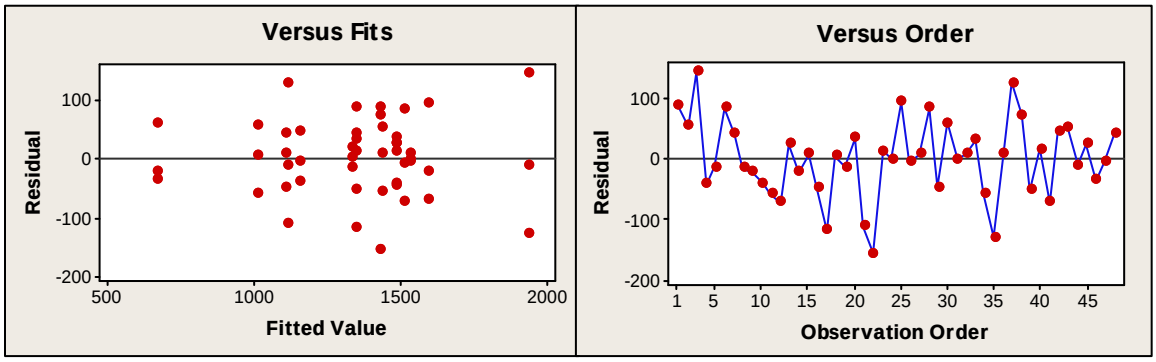

Figure 7: Residual Plots for flexural modulus

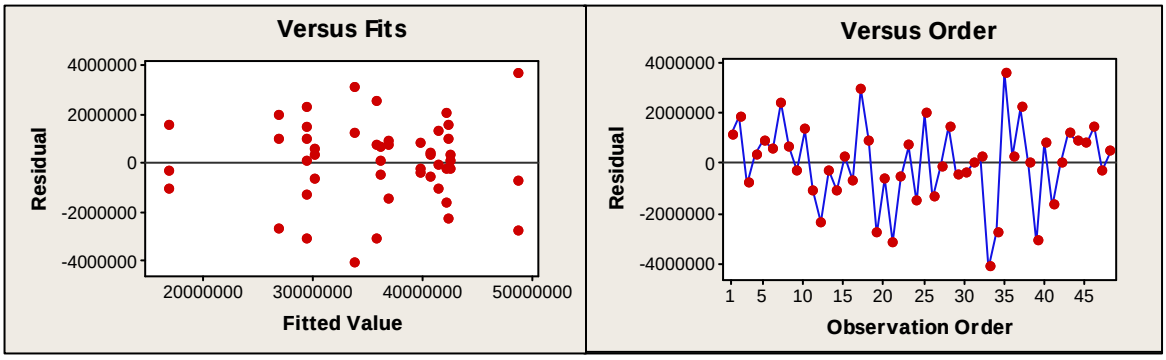

Figure 8: Residual plots for flexural strength

Table 3: Mean Experimental Data

Experiment Id	Width (mm)	Thickness (mm)	Flexural Strength (MPa)	Standard Dev. (MPa)	Flexural Modulus (MPa)	Standard Dev. (MPa)
1	12.89	5.98	33.6	0.40	1117	105.5
2	12.84	5.99	26.7	0.71	1012	56.4
3	13.20	6.06	48.7	6.72	1939	135.8
4	13.65	5.99	40.6	0.03	1482	38.9
5	12.76	5.90	29.4	2.42	1110	118.6
6	12.64	6.08	36.1	0.66	1425	135.3
7	13.05	6.00	35.6	0.69	1348	47.1
8	14.06	6.02	36.8	1.45	1330	16.3
9	13.23	5.82	42.1	0.85	1593	84.1
10	12.64	6.52	29.4	0.37	1154	43.2
11	13.80	6.00	41.3	0.41	1434	55.1
12	12.45	5.98	42.3	1.35	1514	77.9
13	12.66	5.98	39.6	0.26	1482	40.5
14	12.36	6.02	16.7	0.35	666	51.0
15	12.67	6.05	42.4	0.24	1534	6.2
16	12.49	6.02	30.0	0.53	1103	45.8

5.2 Statistical Analysis

Using the experimental data and neglecting aforementioned parameters, a factorial analysis was performed again to determine the effects of a parameter and its interactions on flexural strength and modulus. The resolution V factorial design used will be able to estimate all main effects and all two factor interactions. Thus, the model would produce 16 terms, the intercept term, the 5 main effects, and the 10 two-factor interactions.

The factorial model fitted shows a R^2 and R^2 (adj) value of 95.74% and 93.75% respectively for flexural strength, and 95.25 and 93.03% respectively for flexural modulus, implying a good fit. Normal probability plots were created using the factorial analysis, shown in figure 9. Normal plots are used to graphically convey which main and higher order effects are statistically significant.

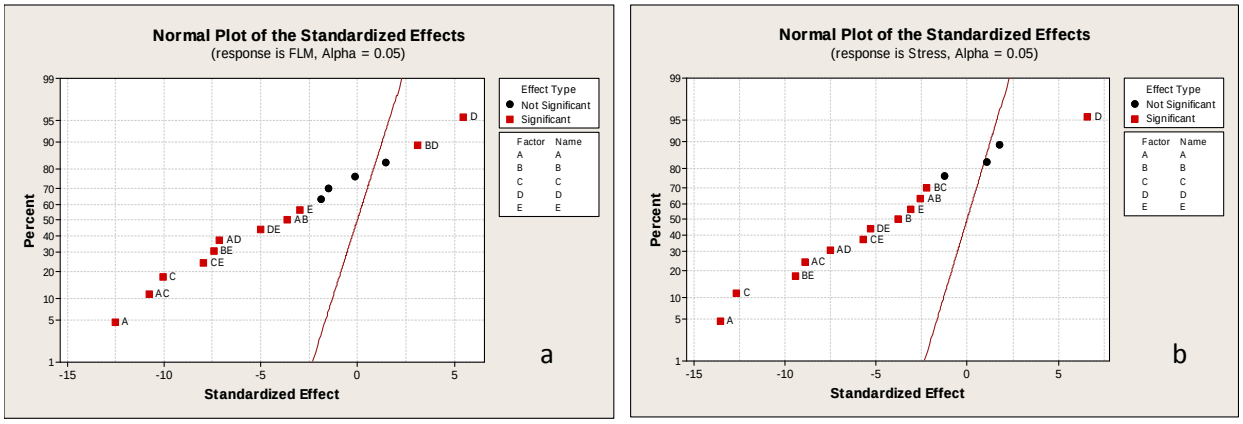

Figure 9: Normal probability plot for (a) flexural modulus and (b) flexural strength

Effects from a consistent process would form a normal distribution, thence statistically significant effects would act as outliers for the dataset. In the plots below statistically significant effects are shown in red boxes whereas insignificant effects are portrayed as black dots.

For flexural strength, the largest absolute effects were air gap and X rotation angle. For second level interactions, the largest absolute effects were air gap*X rotation angle and amplitude/pitch*layer height. Further, all main parameters, i.e., Air Gap, Amplitude/Pitch ratio, Z Rotation angle, X Rotation angle, and Layer Height were found to be statistically significant. Flexural strength increases with increasing Z angle whereas inverse is true for all other parameters. Air gap*Layer Height (A*E), Amplitude/Pitch*Z Rotation angle (B*D), and X Rotation angle* Z Rotation angle (C*D) interactions were statistically insignificant, hence, were removed from further analysis. Similar to flexural strength, for flexural modulus, the largest absolute effects were Air Gap (A) and X rotation angle (C). While, Air gap*X Rotation angle (A*C) had the largest effect for a second level interaction. All main effects except Amplitude/Pitch were statistically significant. Air gap*Layer height (A*E), Amplitude/Pitch *X Rotation angle (B*C), and X Rotation angle* Z Rotation angle (C*D) were found to be statistically insignificant and were neglected from further analysis. However, given Amplitude/Pitch*Layer Thickness (BE) and amplitude/pitch*Z rotation angle are statistically significant for flexural modulus, Amplitude/Pitch cannot be neglect as a parameter. Table 4 and 5 summarize effects of significant variables.

Table 4: Factorial Analysis for Flexural Strength

	Main Effects									
Parameter	**A (Air gap)**		**B (Amplitude/Pitch)**		**C (X rotation angle)**		**D (Z rotation angle)**		**E (Layer height)**	
Parameter level	-1	1	-1	1	-1	1	-1	1	-1	1
Average response	39.6	31.8	36.78	34.62	39.31	32.09	33.82	37.58	36.58	34.82
Effect	-7.741		-2.164		-7.225		3.756		-1.767	
	2nd Order Interactions									
Parameter	**A*B**		**A*C**	**A*D**	**B*C**	**B*E**	**C*E**	**D*E**		
Effect	-1.481		-5.086	-4.299	-1.287	-5.382	-3.252	-3.049		

Table 5: Factorial Analysis for Flexural Modulus

	Main Effects									
Parameter	**A (Air gap)**		**B (Amplitude/Pitch)**		**C (X rotation angle)**		**D (Z rotation angle)**		**E (Layer height)**	
Parameter level	-1	1	-1	1	-1	1	-1	1	-1	1
Average response	1480	1203	1359	1325	1453	1230	1281	1402	1374	1309
Effect	-276.9		-33.5		-223.1		121		-66.1	
	2nd Order Interactions									
Parameter	**A*B**		**A*C**	**A*D**	**B*D**	**B*E**	**C*E**	**D*E**		
Effect	-80.8		-238.3	-157.9	68.5	-164.8	-176.2	-111.2		

5.3 Analysis of Variance (ANOVA)

Analysis of Variance (ANOVA) was performed on the revised factorial design to verify statistical significance of terms and account for variance in strength and modulus. ANOVA is a statistical technique where the sum of squares and error terms are compared against an F-ratio statistic along with p-values to determine the statistical significance of the parameters. The DOE was modeled using least squared sums where the P-value was calculated for each parameter and compared against critical P ratio of 0.05 (95% confidence window) calculated. A summary of ANOVA is shown in table 6 & 7 respectively.

Table 6: ANOVA for Flexural Strength

	Main Effects						
Parameter	**A (Air gap)**	**B (Amplitude/Pitch)**		**C (X rotation angle)**		**D (Z rotation angle)**	**E (Layer height)**
F-value	171.12	13.37		149.07		40.28	8.92
P-value	P<0.001	0.001		P<0.001		P<0.001	0.005
	2nd Order Interactions						
Parameter	**AB**	**AC**	**AD**	**BC**	**BE**	**CE**	**DE**
F-value	6.26	73.87	52.77	4.73	82.73	30.2	26.55
P-value	0.017	P<0.001	P<0.001	0.037	P<0.001	P<0.001	P<0.001

Table 7: ANOVA for Flexural Modulus

	Main Effects						
Parameter	**A (Air gap)**	**B (Amplitude/Pitch)**		**C (X rotation angle)**		**D (Z rotation angle)**	**E (Layer height)**
F-value	145.92	2.13		94.71		27.86	8.31
P-value	P<0.001	0.153		P<0.001		P<0.001	0.007
	2nd Order Interactions						
Parameter	**A*B**	**A*C**	**A*D**	**B*D**	**B*E**	**C*E**	**D*E**
F-value	12.43	108.08	47.45	8.94	51.7	59.05	23.52
P-value	0.001	P<0.001	P<0.001	0.005	P<0.001	P<0.001	P<0.001

5.4 Interaction Effects and interpretation of Analysis of Variance

The authors found that for both flexural strength and flexural modulus all interaction terms had a significant effect on the response and passed statistical significance test in ANOVA. Interaction effect plots were created to validate interactions and if they showed significant effects towards response in the model, figure 10 & 11. Interaction plot show how the relationship between one categorical factor and a continuous response depends on the value of the second categorical factor. Parallel lines indicate no interactions while non-parallel lines show interactions.

Interactions can be divided into ordinal (non-intersection) and disordinal (crossover) interactions. Ordinal interactions have a difference in the mean of each factor for the interaction indicating a main effect of contributing factors as well as an interaction between them. On the other hand, disordinal interactions signify that the mean effect of factor must be qualified in terms of the impact of the second variable and mean effect cannot be interpreted independently. For flexural strength (figure 11) we find that Air gap*Amplitude/Pitch (AB), Air gap*X angle (AC), Air gap*Z angle (AD), Amplitude/Pitch* X angle (BC), X angle*Layer thickness (CE), Z angle*Layer thickness (DE) are ordinal interactions. Additionally, Amplitude/Pitch*layer thickness (B*E) is a disordinal interaction hence the main effects for Amplitude/Pitch ratio (B) and Layer thickness (E) would be ignored.

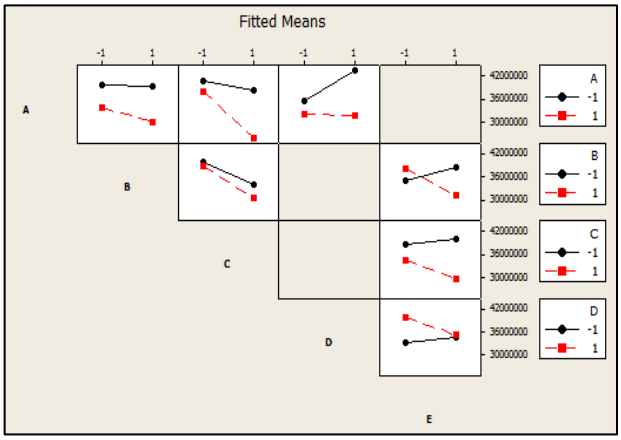

Figure 10: Interaction Plot for Flexural Strength

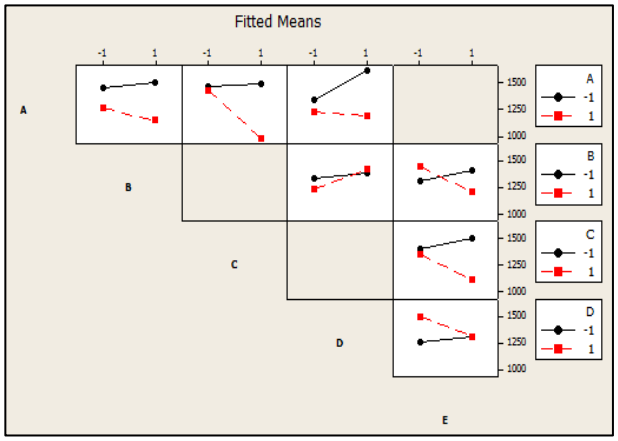

Figure 11: Interaction Plot for Flexural Modulus

In the case of flexural modulus (figure 11), Air gap*Amplitude/Pitch (AB), Air gap*X angle (AC), Air gap*Z angle (AD), X angle*Layer thickness (CE), Z angle*Layer thickness (DE) are ordinal interactions. Amplitude/Pitch* Z angle (BD), Amplitude/Pitch*Layer thickness (BE) on the other hand cross over and are classified as disordinal interactions. Based on these interactions we can conclude that for flexural modulus, main effects for amplitude/pitch and X rotation angle and layer height cannot be interpreted individually. The final effects individually significant for flexural strength and flexural modulus are summarized in table 8.

Table 8: Summary of significant effects for flexural stress and flexural modulus

	Main Effects					2nd order interactions							
Effects	Air gap (A)	Amplitude Pitch Ratio (B)	X Angle (C)	Z Angle (D)	Layer height (E)	AB	AC	AD	BC	BD	BE	CE	DE
Flexural Strength	YES	NO	YES	YES	NO	YES	YES	YES	YES	NO	YES	YES	YES
Flexural Modulus	YES	NO	YES	NO	NO	YES	YES	YES	NO	YES	YES	YES	YES

6. Discussions

6.1 Analysis of Results

From table 5 and figure 10 it can be noted that flexural strength increases for decreasing air gap (A). Air gap is responsible for the decrease in part density due to increased spacing between adjacent roads. Less material is present to bear load, hence, strength decreases. Z rotational angle (D) defines the orientation of high and low sections of a sine wave in the part. This orientation of high and low section of the sine wave have an effect similar to that of raster angle. As raster angle increases the raster length and resistance to bending load decreases however distortion due to thermal gradients also decrease[18]. In case of small rater lengths, the reduction of raster distortion dominates causing an increase in strength[15]. X rotation angle (C) plays an important role in determining the magnitude of shear load acting in the transverse direction from the x-axis of the layer plane. As X rotation angle increases the shear load decreases, load normal to layer increases and strength decreases. This theory is further backed up by the fact fracture surfaces show tensile failure for large X rotation angles.

The amplitude/pitch ratio (B) and layer thickness (E) demonstrate a significant interaction. At higher values of layer thickness, as amplitude/pitch ratio increases the sine function becomes thin and elongated therefore, the number of fully formed sine wavelets in specimen increases resulting in an increase in strength. However, at lower values of layer height the distortion effect coupled with reduced number of fully formed sine waves associated with large amplitude/pitch ratio results in a decrease in strength. But, the increase in diffusion[15] at small layer thickness dominates the interaction between Z rotation angle (D) and layer thickness (E) increasing strength for large values of Z rotation angle and decreasing layer height. It is to be noted that for interaction between air gap (A) and X rotation angle (C), the effect is a combination of increase in density related with small rater angles and large shear forces associated with large X angles resulting in increased strength.

From interaction plots shown in Figure 11, it can be observed that the effect for air gap (A), X rotation angle (C) and Z rotation angle (D) on flexural modulus is similar to what is observed in the case of flexural strength. However, the interaction effects of air gap*amplitude/pitch ratio (AB), air gap*X rotation angle (AC), amplitude/pitch ratio*layer thickness (B*E) and amplitude/pitch ratio*Z rotation angle (BD) show a different behavior. It is known that modulus of stress increases with increasing amplitude/pitch ratio[25], this effect coupled with increased contact area between adjacent rows and layers and full sine wavelets at lower layer heights result in increasing stiffness. Further, increased amplitude/pitch (B) coupled with smaller loads normal to the layer for large Z rotation angle (D) leads to increased flexural modulus. In the case of air gap*amplitude/pitch ratio (A*B) interaction, the effect of amplitude/pitch assisted with increased part density due to small air gap lead to an increase in stiffness of part. Finally, for interaction of air gap*X rotation angle (A*C), increased raster length dominates distortion effects to produce increasing stiffness for small air gap. Based on the analysis presented maximum flexural strength is expected to be found at $A^{-1}B^{-1}C^{-1}D^{1}E^{1}$ and max flexural modulus at A^{-}

$^{1}B^{1}C^{1}D^{1}E^{-1}$. The experimental run for maximum observed flexural modulus was found to coincide with the predicted max flexural strength.

6.3 Sources of Experimental Error

The design of experiment used assumes that the response is purely linear and accounts for variation from the linear trend, however, apart from the given choice and magnitude of parameters used, the response is not likely to be linear. Even though the model used has a good statistical fit (p-value above 90%), replicating experiments with more than 2 levels would be beneficial for an adept understanding of the Active-Z process. Apart from the statistical analysis, the MTS 81-material testing machine used a load cell of 500kN which produced large amounts of noise for small loads used in the testing. A low pass filter was used to minimize noise; however, a more adequate load cell would be better suited. During the test flexural test, crosshead displacement was used to measure maximum central displacement in the specimen which is prone to sag in mechanical linkages. Further, changes in temperature and relative humidity between experiments and testing were not explicitly controlled, affecting the hygroscopic nature of ABS polymers used.

A large variation of size was observed in the as manufactured specimens, in particular for parts with small layer thickness, small Z rotation angle and large X rotation angles. These variation in width can be attributed due to the nozzle geometry rubbing against the part deviating it from the programmed path.

Regression analysis of the main effects produced an R^2 value of 59%. This indicates that either the data is not as linear as expected, or there are parameters that have not been considered. The former is being currently verified with a 3-level design, but requires a significant number of experimental parts and tests. In the case of the latter, additional parameters seen in figure 3 are considered responsible. Though not included for this study, a similar analysis of such additional parameters will be performed in the future. Therefore, this experimental analysis is considered to be part of a larger study to verify factors affecting performance in Active-Z printing and quantify these effects.

7. Closure

The purpose of the study was to investigate the effect of sinusoidal layers on the mechanical properties of parts printed with Active-Z printing and isolate process parameters to study further. The authors employed design of experiments to identify critical factors affecting flexural strength and modulus. The air gap, layer shape, and orientation about the part and layer thickness were varied and statistical analysis found that air gap, X rotation angle and amplitude/pitch ratio were the most significant effect on the tested material properties. Small air gap, small X rotation angles constituted towards stronger parts, while specimens with large amplitude/pitch ratio were found to be stiffer.

This paper provides the framework for future work towards understand effect of repeating sinusoidal structures and their orientation on strength of parts. The authors will study significant parameters to further characterize the shape of a response, and develop a model assist application of this technique towards optimization of mechanical parts. Apart from process characterization, there is a need for a robust slicing algorithm that can effectively calculate layer to part intersection, and produce toolpath that takes strength development in material welds into consideration. An AM process which can vary mechanical properties locally inside a part would add to a designer's ability to develop stronger optimized parts for end use.

8. Acknowledgements

The authors acknowledge Dr. Charles Bakis, Professor of Engineering Sciences and Mechanics at Penn State, for providing access to the MTS 800 for material testing. The authors also acknowledge Joseph Bartolai, PH.D. candidate at Penn State's Center of Innovative Materials Process using Direct Digital Deposition (CIMP-3D), for his assistance with flexural testing. Finally, this project was funded in part by the Pennsylvania State University's College of Engineering Research Initiative (CERI) and Erikson Summer Discovery Grant.

9. References

1. Ahn, Sung-Hoon, Montero, M., Odell, D., Roundy, S., & Wright, P. K "Anisotropic Material Properties of Fused Deposition Modeling ABS." *Rapid Prototyping Journal*, vol. 8, no. 4, Oct. 2002, pp. 248–257.
2. Gibson, I., Rosen, D. W. & Stucker, B. *Additive Manufacturing Technologies: Rapid Prototyping to Direct Digital Manufacturing*, Springer, New York, 2010.
3. ISO/ASTM. *ISO/ASTM 52900-2015: Additive manufacturing -- General principles -- Terminology*. *ISO/ASTM Standards* (2015).
4. Singamneni, Sarat, Asimava Roychoudhury, Olaf Diegel, and Bin Huang. "Modeling and Evaluation of Curved Layer Fused Deposition." *Journal of Materials Processing Technology* 212.1 (2012): 27-35.
5. B. Huang, S. Singamneni, "Curved Layer Fused Deposition Modeling with Varying Raster Orientations", *Applied Mechanics and Materials*, Vols. 446-447, pp. 263-269, 2014.
6. Yerazunis, William S. "Strengthening ABS, Nylon, and Polyester 3D Printed Parts by Stress Tensor Aligned Deposition Paths and Five-Axis Printing." Proceedings of the Solid Freeform Fabrication Symposium, AT&T Conference Center, Austin, Texas. 10 Aug. 2016. Web. 15 Nov. 2016.
7. D. Chakraborty, B. A. Reddy, and R. Choudhury, "Extruder Path Generation for Curved Layer Fused Deposition Modeling," *Computer Aided Design*, Vol. 40, pp. 235-243, 2008.
8. B. Huang, S. Singamneni, "Curved Layer Adaptive Slicing (CLAS) for fused deposition modelling", *Rapid Prototyping Journal*, Vol. 21 Issue: 4, pp. 354-367, 2015
9. Llewellyn-Jones, Thomas, Robert Allen, and Richard Trask. "Curved Layer Fused Filament Fabrication Using Automated Toolpath Generation." *3D Printing and Additive Manufacturing* 3.4 (2016): 236-43.
10. Allen, Robert J., and Richard S. Trask. "An Experimental Demonstration of Effective Curved Layer Fused Filament Fabrication utilizing a Parallel Deposition Robot." *Additive Manufacturing* 8 (2015): 78-87.
11. Lim, Sungwoo, Buswell, Richard A., Valentine, Philip J., Piker, Daniel, Austin, Simon A., and Kestelier, Xavier De. "Modeling Curved-layer Printing Paths for Fabrication Large-scale Construction Components." *Additive Manufacturing* 12 (2016): 216-230. Web.
12. Mohamed, Omar A., Syed H. Masood, and Jahar L. Bhowmik. "Optimization of Fused Deposition Modeling Process Parameters: A Review of Current Research and Future Prospects." *Advances in Manufacturing* 3.1 (2015): 42-53.
13. Said Es, J. Os Foyos, R. Noorani, M. Mandelson, R. Marloth, B.A. Pregger "Effect of layer orientation on mechanical properties of rapid prototyped samples" *Materials and Manufacturing Process* 15 (1) (2000): pp. 107–122.
14. Ziemian, Constance, Mala Sharma, and Sophia Ziemian. "Anisotropic mechanical

properties of ABS parts fabricated by fused deposition modelling". INTECH Open Access Publisher, 2012

15. Sood, Anoop Kumar, R.k. Ohdar, and S.s. Mahapatra. "Parametric Appraisal of Mechanical Property of Fused Deposition Modelling Processed Parts." *Materials & Design*, Vol. 31 Issue: 1, pp.287-95, 2010
16. A.K. Sood, R.K. Ohdar, and S.S. Mahapatra. "Experimental Investigation and Empirical Modelling of FDM Process for Compressive Strength Improvement." *Journal of Advanced Materials*, Vol. 3 Issue: 1, pp.81-90, 2011
17. J. Laeng, Zahid A. Khan and S.Y. Khu, 2006. "Optimizing Flexible Behaviour of Bow Prototype using Taguchi Approach." *Journal of Applied Sciences*, Vol. 6 Issue: 3, pp.622-630, 2006
18. Wang, Ming Tian, Tong Xi Jun, Ye Jin "A Model Research for Prototype Warp Deformation in the FDM Process" *International Journal of Advanced Manufacturing Technology*, Vol 33 Issue 11–12, pp.1087–1096, 2007
19. C.T. Bellehumeur, L. Li, Q. Sun, P. Gu. "Modeling of Bond Formation between Polymer Filaments in the Fused Deposition Modeling Process" *Journal of Manufacturing Processes*, Vol. 6 Issue: 2, pp.170-178, 2004
20. C.T. Bellehumeur, P. Gu, Q. Sun, G.M. Rizvi. "Effect of Processing Conditions on the Bonding Quality of FDM Polymer Filaments" *Rapid Prototyping Journal*, Vol. 14 Issue: 2, pp. 72–80, 2008
21. Bartolai, Joseph, Timothy W. Simpson, and Renxuan Xie. "Predicting Strength of Thermoplastic Polymer Parts Produced using Additive Manufacturing." *Solid Freeform Fabrication Symposium*, Austin, TX. 2016.
22. Page, James Sherwood. "Systems and Methods for Improving 3D Printing". Autodesk, Inc, assignee. Patent US 14/663,393. 24 Sept. 2015. Print.
23. Nick-parker. "Nick-parker/Bread." *GitHub.* 18 May 2016. Web. 28 June 2017.
24. Montgomery, Douglas C. *Design and analysis of experiments*. Hoboken, NJ: John Wiley & Sons, 2007. Print.
25. Yaraghi, Nicholas A., Nicolás Guarín-Zapata, Lessa K. Grunenfelder, Eric Hintsala, Sanjit Bhowmick, Jon M. Hiller, Mark Betts, Edward L. Principe, Jae-Young Jung, Leigh Sheppard, Richard Wuhrer, Joanna Mckittrick, Pablo D. Zavattieri, and David Kisailus. "Biocomposites: A Sinusoidally Architected Helicoidal Biocomposite (Adv. Mater. 32/2016)." *Advanced Materials* 28.32 (2016): 6769. Web.
26. Tam, Kam-Ming Mark, and Caitlin T. Mueller. "Additive Manufacturing along Principal Stress Lines." *3D Printing and Additive Manufacturing* 4.2 (2017): 63-81. Web.